

## Article

# Low Leakage Current and High Breakdown Field AlGaIn/GaN MIS-HEMTs Using PECVD-SiN<sub>x</sub> as a Gate Dielectric

Xiaohui Gao <sup>1</sup>, Hui Guo <sup>1</sup>, Rui Wang <sup>1</sup>, Danfeng Pan <sup>1,2</sup>, Peng Chen <sup>1</sup>, Dunjun Chen <sup>1,\*</sup>, Hai Lu <sup>1</sup>, Rong Zhang <sup>1</sup> and Youdou Zheng <sup>1</sup>

<sup>1</sup> Jiangsu Provincial Key Laboratory of Advanced Photonic and Electronic Materials, School of Electronic Science and Engineering, Nanjing University, Nanjing 210093, China

<sup>2</sup> Microfabrication and Integration Technology Center, Nanjing University, Nanjing 210023, China

\* Correspondence: djchen@nju.edu.cn

**Abstract:** In this paper, SiN<sub>x</sub> film deposited by plasma-enhanced chemical vapor deposition was employed as a gate dielectric of AlGaIn/GaN high electron mobility transistors (HEMTs). We found that the NH<sub>3</sub> flow during the deposition of SiN<sub>x</sub> can significantly affect the performances of metal-insulator-semiconductor (MIS) HEMTs. Compared to that without using NH<sub>3</sub> flow, the device with the optimized NH<sub>3</sub> flow exhibited three orders of magnitude lower gate leakage current, two orders of magnitude higher ON/OFF drain current ratio, and an increased breakdown field by 69%. In addition, an in situ N<sub>2</sub> plasma surface treatment prepared prior to SiN<sub>x</sub> deposition can further improve DC performances of MIS-HEMTs to a very low gate leakage current of 10<sup>-9</sup> mA/mm and a high ON/OFF drain current ratio up to 10<sup>9</sup> by reducing the interface state density. These results demonstrate the great potential for using PECVD-SiN<sub>x</sub> as a gate dielectric in GaN-based MIS-HEMTs.

**Keywords:** PECVD-SiN<sub>x</sub>; AlGaIn/GaN; MIS-HEMTs; in situ plasma treatment; breakdown field



**Citation:** Gao, X.; Guo, H.; Wang, R.; Pan, D.; Chen, P.; Chen, D.; Lu, H.; Zhang, R.; Zheng, Y. Low Leakage Current and High Breakdown Field AlGaIn/GaN MIS-HEMTs Using PECVD-SiN<sub>x</sub> as a Gate Dielectric. *Micromachines* **2022**, *13*, 1396. <https://doi.org/10.3390/mi13091396>

Academic Editor: Giovanni Verzellesi

Received: 6 August 2022

Accepted: 24 August 2022

Published: 26 August 2022

**Publisher's Note:** MDPI stays neutral with regard to jurisdictional claims in published maps and institutional affiliations.



**Copyright:** © 2022 by the authors. Licensee MDPI, Basel, Switzerland. This article is an open access article distributed under the terms and conditions of the Creative Commons Attribution (CC BY) license (<https://creativecommons.org/licenses/by/4.0/>).

## 1. Introduction

Gallium nitride-based HEMTs have been considered excellent candidates for next-generation high-efficiency power switching devices due to their remarkable material and transport properties. However, conventional Schottky-gate HEMTs have a large gate leakage current and a small gate swing, which are limited by the Schottky-gate forward turn-on voltage (e.g., <3 V) [1,2]. To mitigate these issues, MIS-HEMTs have been proposed. It can suppress gate leakage and improve gate reliability by inserting an insulator between the gate metal and the barrier layer. Various dielectric materials are suitable as gate insulators, such as SiO<sub>2</sub> [3], SiN<sub>x</sub> [4–10], Al<sub>2</sub>O<sub>3</sub> [11,12], and SiON [13]. Among them, nitride-based gate dielectrics (e.g., SiN<sub>x</sub>) can avoid the additional introduction of interfacial Ga-O bonds, which tend to introduce interface traps and cause threshold voltage instability [4,14–17]. Currently, SiN<sub>x</sub> has been widely used as a gate dielectric/interfacial gate dielectric. There are many methods to deposit SiN<sub>x</sub>, such as plasma-enhanced chemical vapor deposition (PECVD) [1,18], low-pressure chemical vapor deposition (LPCVD) [4–6,8], and metal-organic chemical vapor deposition (MOCVD) [7,9].

Deposition methods, deposition conditions, and surface treatment before dielectric deposition can significantly affect the properties of SiN<sub>x</sub> films. Recently, LPCVD has been reported as a possible alternative technique for depositing high-quality SiN<sub>x</sub> [4–6,8]. However, dielectric deposition at a very high temperature is not compatible with typical microelectronic interconnect processing and may create surface defects due to the decomposition of GaN above 650 °C [19]. In situ SiN<sub>x</sub> grown by MOCVD may have Si contamination in the MOCVD chamber [5]. Compared with these gate dielectric deposition methods, using plasma-enhanced chemical vapor deposition (PECVD) SiN<sub>x</sub> shows great advantages in low temperature, easy operation, and high deposition rate [20–22]. PECVD-grown SiN<sub>x</sub>

has been proven to be an effective material to suppress current collapse and reduce the surface states in AlGaN/GaN HEMTs.

In this work, we investigated the influence of SiN<sub>x</sub> deposition condition and surface treatment on the electrical properties of GaN-based MIS-HEMTs employing PECVD-SiN<sub>x</sub> as the gate dielectric. To evaluate the dielectric quality and interface properties, current–voltage (I–V) characterization, X-ray photoelectron spectroscopy (XPS), and capacitance–voltage (C–V) measurements were performed. The results showed that the optimized device exhibits a lower leakage current, a higher ON/OFF drain current, and a higher breakdown field than the device without any optimization.

## 2. Device Fabrication

To improve the breakdown field of the SiN<sub>x</sub> dielectric, we first optimized the deposition conditions of SiN<sub>x</sub> on Pt substrates using plasma-enhanced chemical vapor deposition by changing the flow of NH<sub>3</sub>. The reactant precursors were SiH<sub>4</sub> (5%)/N<sub>2</sub>, NH<sub>3</sub> and N<sub>2</sub>. The as-deposited 100 nm SiN<sub>x</sub> films were fabricated into metal–semiconductor–metal (MIM) capacitors for the measurements of breakdown field strength. The flow of NH<sub>3</sub> was varied with a fixed SiH<sub>4</sub>: N<sub>2</sub> ratio, a chamber pressure (=600 mtorr), and an RF power of 10 W. The results showed that NH<sub>3</sub> flow could significantly affect the breakdown field of SiN<sub>x</sub> films, as presented in Figure 1a, and finally a maximum breakdown field of 11.45 MV/cm, which exceeds the reported breakdown field strength of PECVD-SiN<sub>x</sub> as a gate dielectric, was obtained at the condition of NH<sub>3</sub> flow of 40 sccm.

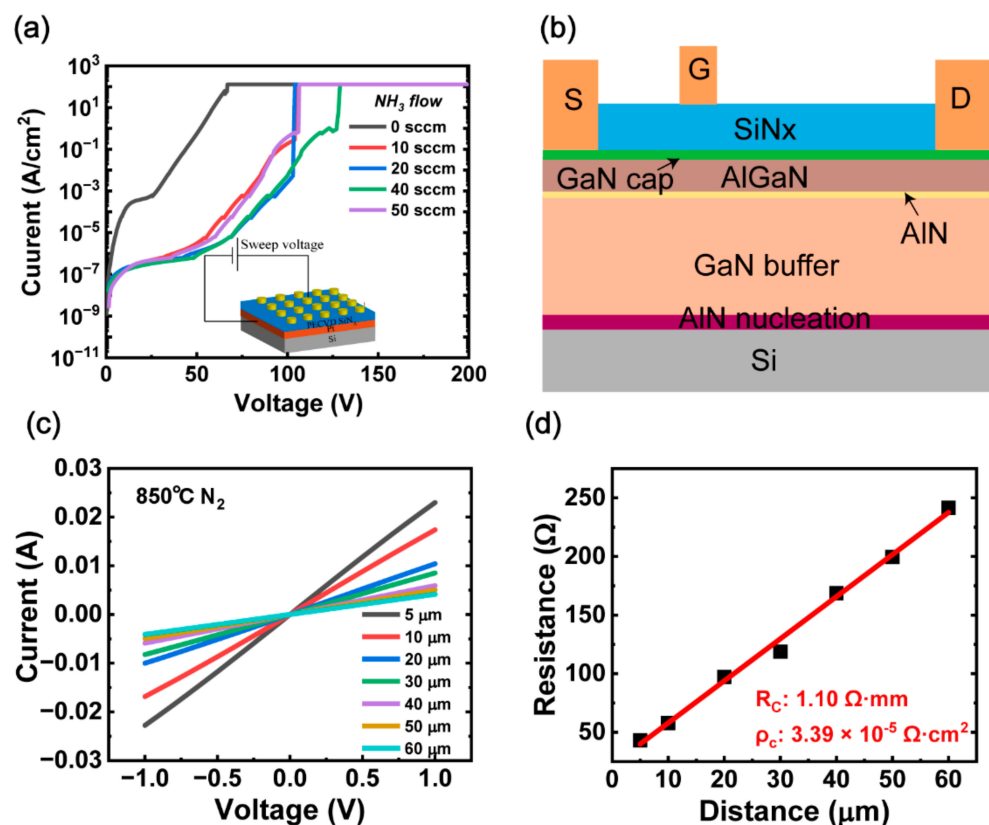


**Figure 1.** (a) Forward leakage current characteristics for circular MIM patterns with a 100  $\mu\text{m}$  diameter. (b) Schematic cross-sectional view of fabricated PECVD-SiN<sub>x</sub> MIS-HEMTs. (c) I–V characteristics of a TLM structure of Ti/Al/Ni/Au contacts after annealing at 850  $^{\circ}\text{C}$  in N<sub>2</sub> ambient. (d) Extracted resistance versus TLM distance.

The AlGaN/GaN heterostructure was grown by MOCVD on a silicon substrate. The epitaxial structure consisted of a 1-nm GaN cap layer, a 15-nm AlGaN barrier layer, a 1-nm AIN layer, a 4- $\mu\text{m}$  GaN buffer layer, and an AIN nucleation layer, as shown schematically

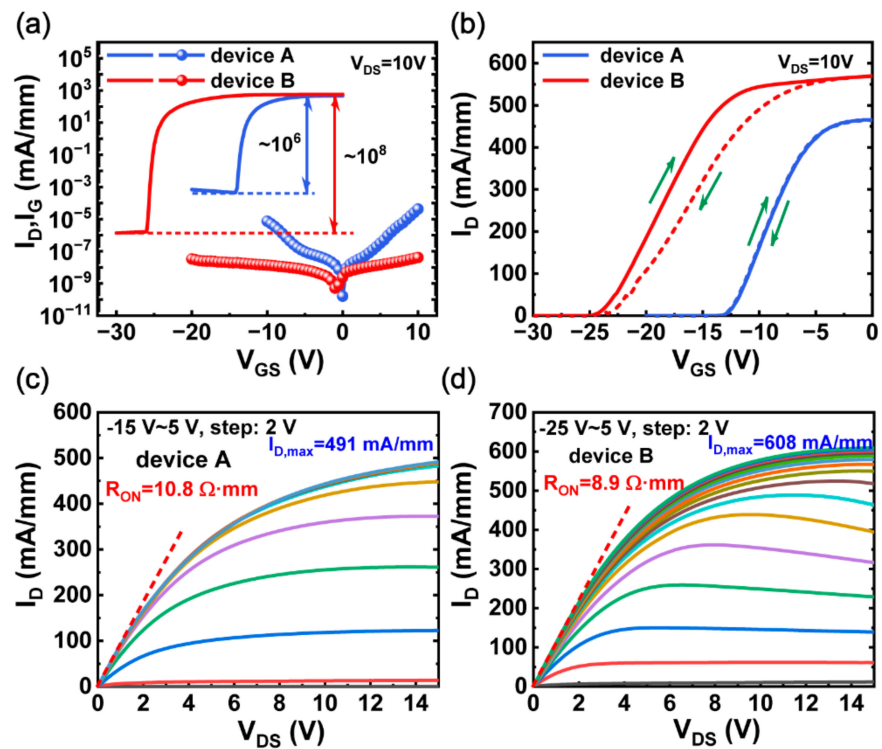
in Figure 1b. The use of AlN nucleation layer can release the tensile stress and reduce the dislocation defects on the epitaxial surface of GaN, thus improving the crystalline quality of GaN and reducing the cracking [23,24]. The device-fabrication started with electron beam evaporation of Ti/Al/Ni/Au and alloyed at 850 °C for 30 s in a N<sub>2</sub> atmosphere to form an ohmic contact. The value of specific contact resistivity ( $\rho_c$ ) of the ohmic contact was  $3.39 \times 10^{-5} \Omega \cdot \text{cm}^2$ , as seen in Figure 1c,d [25,26]. Subsequently, a mesa isolation process was implemented by an inductively coupled plasma (ICP) system using a BCl<sub>3</sub>/Cl<sub>2</sub> gas mixture. After that, 30-nm SiN<sub>x</sub> under the condition without NH<sub>3</sub> gas was deposited for sample A and 30-nm SiN<sub>x</sub> under the condition with 40 sccm NH<sub>3</sub> was deposited for sample B. Considering the effect of surface treatment, an in situ N<sub>2</sub> plasma treatment before SiN<sub>x</sub> deposition, with NH<sub>3</sub> gas flow of 40 sccm, was employed for sample C. The Ni/Au (50/100 nm) gate metal was then deposited by E-beam evaporation. Finally, the contact window was opened by a reactive ion etching (RIE) dry-etching system. The gate-to-source space is 4 μm, the gate-to-drain space is 12 μm, and the gate width and length are 100 μm and 4 μm, respectively. The fabricated devices were marked device A, B, and C, corresponding sample A, B, and C, respectively.

### 3. Results and Discussion

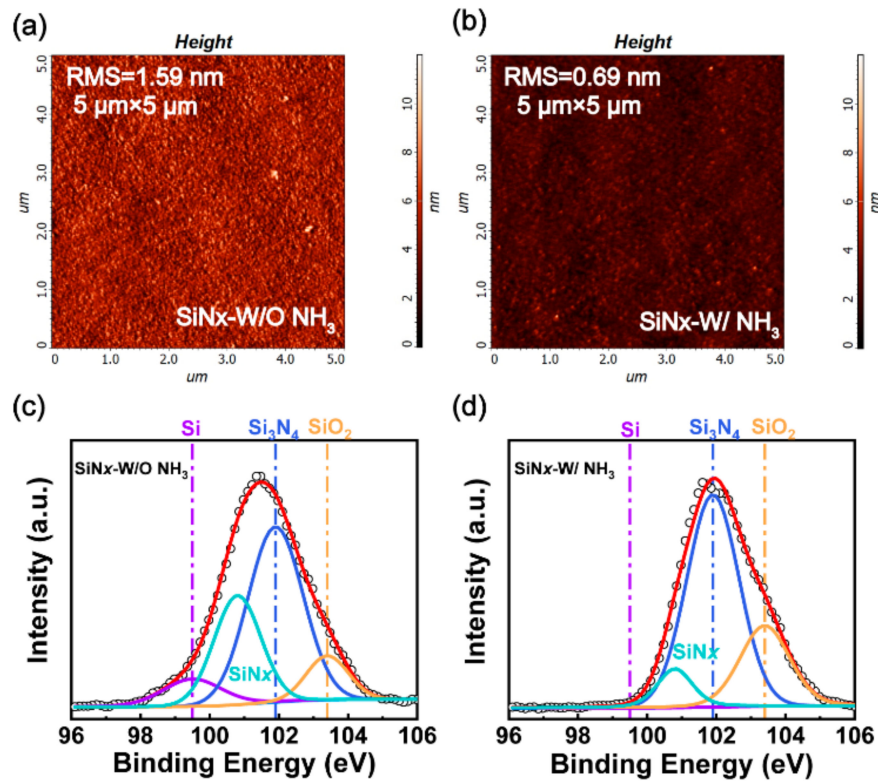
#### 3.1. Material Optimization Characteristics

Figure 2 shows typical DC transfer, gate leakage, and output characteristics of PECVD-SiN<sub>x</sub>/AlGaIn/GaN MIS-HEMTs. The transfer characteristics of MIS-HEMTs were measured at a drain bias voltage of 10 V. Compared with device A, device B exhibits a much higher ON/OFF drain current ratio of  $\sim 10^8$ . In addition, device B shows a very low gate leakage current of  $\sim 10^{-8}$  mA/mm at both  $V_G = -20$  V and  $V_G = 10$  V, three orders of magnitude lower than that of device A, suggesting that SiN<sub>x</sub> deposition with NH<sub>3</sub> flow can effectively suppress leakage paths in the gate dielectric. In Figure 2b, device B shows a relatively larger threshold voltage hysteresis, compared with device A. This indicates that SiN<sub>x</sub> without NH<sub>3</sub> can alleviate the surface trapping effect. Meanwhile, a large negative threshold voltage shift in device B may come from the high density of positive charges existing at the interface between SiN<sub>x</sub> and AlGaIn [27]. In addition, these positive charges may be introduced by the hydrogen radicals originating from NH<sub>3</sub>. As shown in Figure 2c,d, device B shows a larger saturated output current of 608 mA/mm and a lower on-resistance of 8.9 Ω·mm, compared with device A.

To further understand the reasons for the improved electrical performances obtained by optimizing the NH<sub>3</sub> flow, we analyzed the dielectric surface roughness and the N/Si ratio of SiN<sub>x</sub> with different deposition conditions by employing atomic force microscopy (AFM) and X-ray photoelectron spectroscopy (XPS). As shown in Figure 3a,b, the root mean square (RMS) roughness over a 5 μm × 5 μm area is 1.59 nm for SiN<sub>x</sub> without NH<sub>3</sub>, but 0.69 nm for SiN<sub>x</sub> with 40 sccm NH<sub>3</sub>, indicating that NH<sub>3</sub> can effectively reduce the surface roughness of the SiN<sub>x</sub> dielectric. Typical Si 2p core-level spectrums were captured as shown in Figure 3c,d. Three components corresponding to Si-Si bonds, Si-N bonds, and Si-O bonds were extracted from the spectrum. The amount of elemental composition incorporation in SiN<sub>x</sub> was estimated in Table 1 by using the standard method, as reported in Ref. [28]. The SiN<sub>x</sub> stoichiometry ( $x = [\text{N}]/[\text{Si}]$ ) was analyzed by the peak area sensitivity method [29], and the results showed that the corresponding N/Si ratio was changed from 0.75 to 1.05 before and after optimizing NH<sub>3</sub> flow, respectively. Moreover, with the increase in N/Si ratio, the Si-Si bond contents decreased while the Si-O bond and Si-N bond contents increased. An increase in the N/Si ratio was demonstrated to be able to improve the insulation characteristics of the SiN<sub>x</sub> dielectric film, as reported in Refs. [27,30], which can explain why device B exhibits better DC characteristics than device A.



**Figure 2.** (a) Transfer and gate leakage characteristics of device A and B on a log scale. (b) Transfer characteristics of device A and B on a linear scale. Output characteristics of (c) device A and (d) device B. Device dimensions:  $L_{GS}/L_{GD}/L_G/W_G = 4/12/4/100 \mu\text{m}$ .



**Figure 3.** AFM images of the SiNx surface in (a) device A and (b) device B within a  $5 \mu\text{m} \times 5 \mu\text{m}$  area. Fitting XPS results of the Si 2p core-level spectrum of (c) the SiNx film without NH<sub>3</sub> gas and (d) the SiNx with an NH<sub>3</sub> gas flow of 40 sccm.

**Table 1.** The elemental composition of SiN<sub>x</sub> grown by PECVD.

Samples	Si	N	N/Si
SiN <sub>x</sub> -W/O NH <sub>3</sub>	34.43	25.7	0.75
SiN <sub>x</sub> -W/NH <sub>3</sub>	28.1	29.52	1.05

### 3.2. Interface Optimization Characteristics

However, device B shows a larger voltage hysteresis than device A, which may result from hydrogen radicals originating from NH<sub>3</sub>. It has been confirmed that NH<sub>3</sub> can diffuse into the GaN structure and react with Ga-N bonds, thus resulting in the generation of nitrogen vacancies and Ga-H bonds near the surface [31,32]. To reduce these interface defects, some surface treatment methods have been well developed [33–37]. In this work, an in situ N<sub>2</sub> plasma surface treatment was adopted before dielectric deposition for device C which has the same subsequent processes as device B. As shown in Figure 4a,b, device A shows the smallest V<sub>TH</sub> hysteresis and the lowest ON/OFF drain current ratio. In addition, it can be seen that the saturation current in device A is the smallest, indicating that device A has the lowest 2DEG concentration at the AlGaIn/GaN interface. Device C exhibits a large positive shift of V<sub>TH</sub> compared to device B, which may be related to the reduction of nitrogen-vacancy defects, thus reducing the positive charges [34]. Meanwhile, the transconductance and ON/OFF drain current ratio (~10<sup>9</sup>) of device C are further improved, indicating that in situ N<sub>2</sub> plasma treatment can suppress the trapping of channel carriers by surface defects. Moreover, device C exhibits the lowest ON-resistance of 7.9 Ω·mm and the highest saturation output current up to 650 mA/mm in comparison with device A and B, which can be attributed to the improvement of field-effect mobility. As presented in Figure 4d, device C shows the highest field-effect mobility because of the improvement in device transconductance, thus reducing the on-resistance in device C. Since the on-resistance is mainly related to field-effect mobility and carrier concentration, device A has the largest on-resistance. Generally, after optimization, the maximum drain current and the field-effect mobility of device C increased by 32% and 28%, respectively, compared with device A.

Furthermore, the gate leakage characteristics of the MIS-HEMTs were measured at V<sub>DS</sub> = 0 V as shown in Figure 5. In comparison with device A, device B and C exhibit much lower gate leakage current and higher forward gate breakdown voltage up to 34 V at room temperature due to the optimized deposition condition of the SiN<sub>x</sub> dielectric with NH<sub>3</sub> flow. The corresponding electric field strength (E<sub>b</sub>) was estimated to be 11 MV/cm, a very competitive result referring to those of reported MIS-HEMTs. We benchmarked the gate leakage current versus electrical field against these reported AlGaIn/GaN MIS-HEMTs [3–13,38], as plotted in Figure 5b. In general, the gate leakage and breakdown field of the optimized device in this work are comparable to those of the reported state-of-the-art AlGaIn/GaN MIS-HEMTs.

Finally, capacitance–voltage (C–V) measurements were performed on the MIS diodes, corresponding to device B and C, with different frequencies varying from 20 kHz to 1 MHz at room temperature. As shown in Figure 6, there are two obvious steps in both C–V curves. The first step corresponds to the process of accumulating two-dimensional electron gas in the AlGaIn/GaN heterojunction while the second step reflects the electron transfer from the AlGaIn/GaN to the SiN<sub>x</sub>/GaN interfaces [39]. In comparison with device B, device C exhibits a smaller frequency dispersion in the second step, indicating a higher quality interface of SiN<sub>x</sub>/GaN that has a lower trap density. We also calculated the interface state density using the method in Ref. [40], and the results are shown in Figure 6c. We found that the interface state density was reduced by almost one order of magnitude after the in situ N<sub>2</sub> plasma surface treatment indicating that nitrogen vacancies and surface oxygen-related bonds can be effectively reduced by an in situ N<sub>2</sub> plasma treatment, thus obtaining a high-quality SiN<sub>x</sub>/GaN interface.

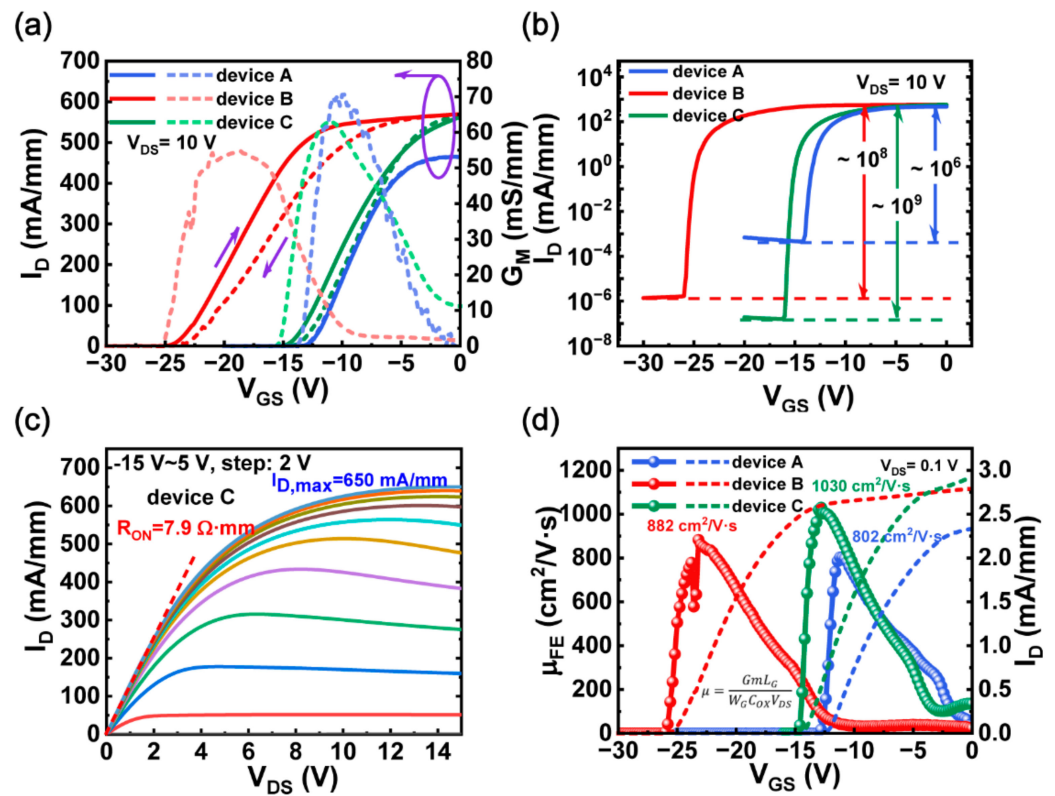


**Figure 4.** Transfer characteristics of device A, B, and C on the (a) linear scale and (b) log scale. (c) Output characteristics of device C. Device dimensions:  $L_{GS}/L_{GD}/L_G/W_G = 4/12/4/100 \mu\text{m}$ . (d) Extracted field-effect mobility using a long-channel device with  $L_G/W_G = 40/100 \mu\text{m}$  at  $V_{DS} = 0.1 \text{ V}$ .

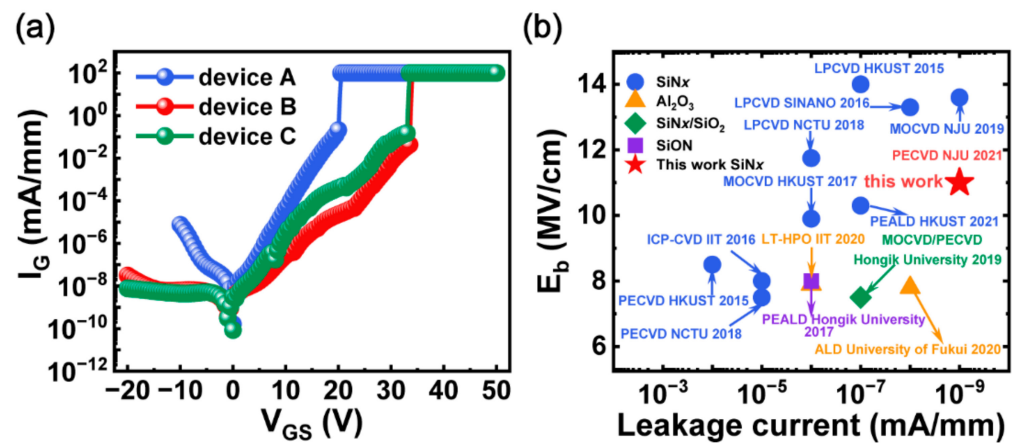


**Figure 5.** (a)  $I_G - V_{GS}$  characteristics of PECVD-SiNx/AlGaIn/GaN MIS-HEMTs. Device dimensions:  $L_{GS}/L_{GD}/L_G/W_G = 4/12/4/100 \mu\text{m}$ . (b) Benchmark of leakage current versus electrical field in recent reports [3–13,38].

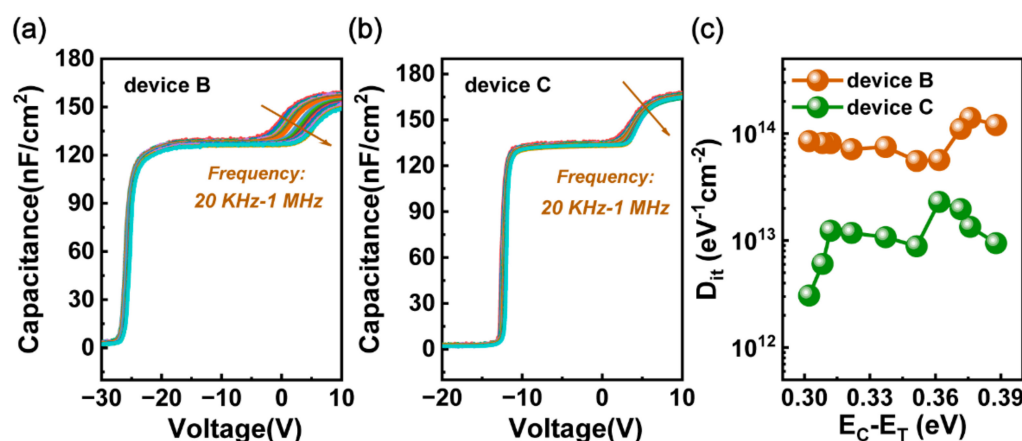


**Figure 6.** C–V characteristics of (a) device B and (b) device C with frequencies varying from 20 kHz to 1 MHz. (c) Trap density as a function of energy level for device B and C.

#### 4. Conclusions

In summary, we studied the impact of SiN<sub>x</sub> growth condition and surface treatment on the electrical properties of AlGa<sub>N</sub>/Ga<sub>N</sub> MIS-HEMTs when employing PECVD-SiN<sub>x</sub> as a gate dielectric. The results show that the gate leakage current can be greatly suppressed by increasing the N/Si ratio of SiN<sub>x</sub>, and the interface state density can be obviously reduced through in situ N<sub>2</sub> plasma surface treatment. The optimized SiN<sub>x</sub>/AlGa<sub>N</sub>/Ga<sub>N</sub> MIS-HEMTs exhibit low gate leakage current, high I<sub>ON</sub>/I<sub>OFF</sub> ratio, and high breakdown field. These results prove that PECVD-SiN<sub>x</sub>/AlGa<sub>N</sub>/Ga<sub>N</sub> MIS-HEMT is comparable to those of the reported state-of-the-art AlGa<sub>N</sub>/Ga<sub>N</sub> MIS-HEMTs.

**Author Contributions:** Methodology, X.G.; investigation, X.G.; validation, H.G. and R.W.; writing—original draft preparation, X.G.; writing—review and editing, D.C.; supervision, D.P., P.C., H.L., R.Z. and Y.Z.; funding acquisition, D.C., D.P. and H.G. All authors have read and agreed to the published version of the manuscript.

**Funding:** This work was supported by the State Key R&D Project of Jiangsu Province, China (BE2022070-4, BE2021026), the National Natural Science Foundation of China (62104096) and China Postdoctoral Science Foundation (2022TQ0142).

**Conflicts of Interest:** The authors declare no conflict of interest.

#### References

1. Tang, Z.; Jiang, Q.; Lu, Y.; Huang, S.; Yang, S.; Tang, X.; Chen, K.J. 600-V normally off SiN<sub>x</sub>/AlGa<sub>N</sub>/Ga<sub>N</sub> MIS-HEMT with large gate swing and low current collapse. *IEEE Electron Device Lett.* **2013**, *34*, 1373–1375. [\[CrossRef\]](#)
2. Hernández-Gutiérrez, C.A.; Kudriavtsev, Y.; Cardona, D.; Hernández, A.G.; Camas-Anzueto, J.L. Optical, electrical, and chemical characterization of nanostructured In<sub>x</sub>Ga<sub>1-x</sub>N formed by high fluence In<sup>+</sup> ion implantation into Ga<sub>N</sub>. *Opt. Mater.* **2021**, *111*, 110541. [\[CrossRef\]](#)
3. Cho, G.; Cha, H.Y.; Kim, H. Influence of Oxygen-Plasma Treatment on In-Situ SiN/AlGa<sub>N</sub>/Ga<sub>N</sub> MOSHEMT with PECVD SiO<sub>2</sub> Gate Insulator. *Materials* **2019**, *12*, 3968. [\[CrossRef\]](#) [\[PubMed\]](#)
4. Hua, M.; Liu, C.; Yang, S.; Liu, S.; Fu, K.; Dong, Z.; Cai, Y.; Zhang, B.; Chen, K.J. Characterization of Leakage and Reliability of SiN<sub>x</sub> Gate Dielectric by Low-Pressure Chemical Vapor Deposition for Ga<sub>N</sub>-based MIS-HEMTs. *IEEE Trans. Electron Devices* **2015**, *62*, 3215–3222. [\[CrossRef\]](#)
5. Hua, M.; Liu, C.; Yang, S.; Liu, S.; Fu, K.; Dong, Z.; Cai, Y.; Zhang, B.; Chen, K.J. Ga<sub>N</sub>-Based Metal-Insulator-Semiconductor High-Electron-Mobility Transistors Using Low-Pressure Chemical Vapor Deposition SiN<sub>x</sub> as Gate Dielectric. *IEEE Electron Device Lett.* **2015**, *36*, 448–450. [\[CrossRef\]](#)
6. Zhang, Z.; Yu, G.; Zhang, X.; Deng, X.; Li, S.; Fan, Y.; Sun, S.; Song, L.; Tan, S.; Wu, D.; et al. Studies on High-Voltage Ga<sub>N</sub>-on-Si MIS-HEMTs Using LPCVD Si<sub>3</sub>N<sub>4</sub> as Gate Dielectric and Passivation Layer. *IEEE Trans. Electron Devices* **2016**, *63*, 731–738. [\[CrossRef\]](#)
7. Jiang, H.; Liu, C.; Chen, Y.; Lu, X.; Tang, C.W.; Lau, K.M. Investigation of In Situ SiN as Gate Dielectric and Surface Passivation for Ga<sub>N</sub> MISHEMTs. *IEEE Trans. Electron Devices* **2017**, *64*, 832–839. [\[CrossRef\]](#)
8. Wang, H.-C.; Lumbantoruan, F.J.; Hsieh, T.-E.; Wu, C.-H.; Lin, Y.-C.; Chang, E.Y. High-Performance LPCVD-SiN<sub>x</sub>/InAlGa<sub>N</sub>/Ga<sub>N</sub> MIS-HEMTs with 850-V 0.98-mΩ·cm<sup>2</sup> for Power Device Applications. *IEEE J. Electron Devices Soc.* **2018**, *6*, 1136–1141. [\[CrossRef\]](#)

9. Cheng, L.; Xu, W.; Pan, D.; Liang, H.; Wang, R.; Zhu, Y.; Ren, F.; Zhou, D.; Ye, J.; Chen, D.; et al. Gate-first AlGa<sub>N</sub>/Ga<sub>N</sub> HEMT technology for enhanced threshold voltage stability based on MOCVD-grown in situ Si<sub>3</sub>N<sub>4</sub>. *J. Phys. D Appl. Phys.* **2021**, *54*, 015105. [[CrossRef](#)]
10. Dutta, G.; DasGupta, N.; DasGupta, A. Low-Temperature ICP-CVD Si<sub>3</sub>N<sub>4</sub> as Gate Dielectric for Ga<sub>N</sub>-Based MIS-HEMTs. *IEEE Trans. Electron Devices* **2016**, *63*, 4693–4701. [[CrossRef](#)]
11. Asubar, J.T.; Kawabata, S.; Tokuda, H.; Yamamoto, A.; Kuzuhara, M. Enhancement-Mode AlGa<sub>N</sub>/Ga<sub>N</sub> MIS-HEMTs with High V<sub>TH</sub> and High I<sub>Dmax</sub> Using Recessed-Structure with Regrown AlGa<sub>N</sub> Barrier. *IEEE Electron Device Lett.* **2020**, *41*, 693–696. [[CrossRef](#)]
12. Kanaga, S.; Dutta, G.; Kushwah, B.; DasGupta, N.; DasGupta, A. Low Temperature and High Pressure Oxidized Al<sub>2</sub>O<sub>3</sub> as Gate Dielectric for AlInN/GaN MIS-HEMTs. *IEEE Trans. Device Mater. Reliab.* **2020**, *20*, 613–621. [[CrossRef](#)]
13. Kim, H.-S.; Han, S.-W.; Jang, W.-H.; Cho, C.-H.; Seo, K.-S.; Oh, J.; Cha, H.-Y. Normally-off Ga<sub>N</sub>-on-Si MISFET Using PECVD Si<sub>3</sub>N<sub>4</sub> Gate Dielectric. *IEEE Electron Device Lett.* **2017**, *38*, 1090–1093. [[CrossRef](#)]
14. Huang, S.; Yang, S.; Roberts, J.; Chen, K.J. Threshold Voltage Instability in Al<sub>2</sub>O<sub>3</sub>/Ga<sub>N</sub>/AlGa<sub>N</sub>/Ga<sub>N</sub> Metal-Insulator-Semiconductor High-Electron Mobility Transistors. *Jpn. J. Appl. Phys.* **2011**, *50*, 110202. [[CrossRef](#)]
15. Lu, Y.; Yang, S.; Jiang, Q.; Tang, Z.; Li, B.; Chen, K.J. Characterization of V<sub>T</sub>-instability in enhancement-mode Al<sub>2</sub>O<sub>3</sub>-AlGa<sub>N</sub>/Ga<sub>N</sub> MIS-HEMTs. *Phys. Status Solidi C* **2013**, *10*, 1397–1400. [[CrossRef](#)]
16. Ma, X.-H.; Zhu, J.-J.; Liao, X.-Y.; Yue, T.; Chen, W.-W.; Hao, Y. Quantitative characterization of interface traps in Al<sub>2</sub>O<sub>3</sub>/AlGa<sub>N</sub>/Ga<sub>N</sub> metal-oxide-semiconductor high-electron-mobility transistors by dynamic capacitance dispersion technique. *Appl. Phys. Lett.* **2013**, *103*, 033510. [[CrossRef](#)]
17. Yang, S.; Tang, Z.; Wong, K.-Y.; Lin, Y.-S.; Liu, C.; Lu, Y.; Huang, S.; Chen, K.J. High-Quality Interface in Al<sub>2</sub>O<sub>3</sub>/Ga<sub>N</sub>/AlGa<sub>N</sub>/Ga<sub>N</sub> MIS Structures with In Situ Pre-Gate Plasma Nitridation. *IEEE Electron Device Lett.* **2013**, *34*, 1497–1499. [[CrossRef](#)]
18. Hove, M.V.; Boulay, S.; Bahl, S.R.; Stoffels, S.; Kang, X.; Wellekens, D.; Geens, K.; Delabie, A.; Decoutere, S. CMOS Process-Compatible High-Power Low-Leakage AlGa<sub>N</sub>/Ga<sub>N</sub> MISHEMT on Silicon. *IEEE Electron Device Lett.* **2012**, *33*, 667–669. [[CrossRef](#)]
19. Maier, D.; Alomari, M.; Grandjean, N.; Carlin, J.-F.; Diforte-Poisson, M.-A.; Dua, C.; Chuvilin, A.; Troadec, D.; Gaquiere, C.; Kaiser, U.; et al. Testing the Temperature Limits of Ga<sub>N</sub>-Based HEMT Devices. *IEEE Trans. Device Mater. Reliab.* **2010**, *10*, 427–436. [[CrossRef](#)]
20. Yota, J.; Hander, J.; Saleh, A.A. A comparative study on inductively-coupled plasma high-density plasma, plasma-enhanced, and lowpressure chemical vapor deposition silicon nitride films. *J. Vac. Sci. Technol. A* **2000**, *18*, 372–376. [[CrossRef](#)]
21. Guler, I. Optical and structural characterization of silicon nitride thin films deposited by PECVD. *Mater. Sci. Eng. B* **2019**, *246*, 21–26. [[CrossRef](#)]
22. Piccirillo, A.; Gobbi, A.L. Physical-Electrical Properties of Silicon Nitride Deposited by PECVD on III–V Semiconductors. *J. Electrochem. Soc.* **1990**, *137*, 3910–3917. [[CrossRef](#)]
23. Zambrano-Serrano, M.A.; Hernández, C.A.; de Melo, O.; Behar, M.; Gallardo-Hernández, S.; Casallas-Moreno, Y.L.; Ponce, A.; Hernandez-Robles, A.; Bahena-Urbe, D.; Yee-Rendón, C.M.; et al. Effects of heavy Si doping on the structural and optical properties of n-GaN/AlN/Si(111) heterostructures. *Mater. Res. Express* **2022**, *9*, 065903. [[CrossRef](#)]
24. Pan, L.; Dong, X.; Li, Z.; Luo, W.; Ni, J. Influence of the AlN nucleation layer on the properties of AlGa<sub>N</sub>/Ga<sub>N</sub> heterostructure on Si (1 1 1) substrates. *Appl. Surf. Sci.* **2018**, *447*, 512–517. [[CrossRef](#)]
25. Greco, G.; Prystawko, P.; Leszczyński, M.; Lo Nigro, R.; Raineri, V.; Roccaforte, F. Electro-structural evolution and Schottky barrier height in annealed Au/Ni contacts onto p-GaN. *J. Appl. Phys.* **2011**, *110*, 123703. [[CrossRef](#)]
26. Hernández-Gutiérrez, C.A.; Kudriavtsev, Y.; Mota, E.; Hernández, A.G.; Escobosa-Echavarría, A.; Sánchez-Resendiz, V.; Casallas-Moreno, Y.L.; López-López, M. A new method of making ohmic contacts to p-GaN. *Nucl. Instrum. Methods Phys. Res. B* **2016**, *388*, 35–40. [[CrossRef](#)]
27. Huang, T.; Jiang, H.; Bergsten, J.; Lau, K.M.; Rorsman, N. Enhanced gate stack stability in Ga<sub>N</sub> transistors with gate dielectric of bilayer Si<sub>3</sub>N<sub>4</sub> by low pressure chemical vapor deposition. *Appl. Phys. Lett.* **2018**, *113*, 232102. [[CrossRef](#)]
28. Nayak, S.K.; Gupta, M.; Shivaprasad, S.M. Structural, optical and electronic properties of a Mg incorporated Ga<sub>N</sub> nanowall network. *RSC Adv.* **2017**, *7*, 25998–26005. [[CrossRef](#)]
29. Siddique, A.; Ahmed, R.; Anderson, J.; Holtz, M.; Piner, E.L. Improved Electrical Properties of AlGa<sub>N</sub>/Ga<sub>N</sub> High-Electron-Mobility Transistors by In Situ Tailoring the Si<sub>3</sub>N<sub>4</sub> Passivation Layer. *ACS Appl. Mater. Interfaces* **2021**, *13*, 18264–18273. [[CrossRef](#)]
30. Gupta, M.; Rathi, V.K.; Thangaraj, R.; Agnihotri, O.P. The preparation, properties and applications of silicon nitride thin films deposited by plasma-enhanced chemical vapor deposition. *Thin Solid Films* **1991**, *204*, 77–106. [[CrossRef](#)]
31. Hashizume, T.; Nakasaki, R. Discrete surface state related to nitrogen-vacancy defect on plasma-treated Ga<sub>N</sub> surfaces. *Appl. Phys. Lett.* **2002**, *80*, 4564–4566. [[CrossRef](#)]
32. Puzyrev, Y.S.; Roy, T.; Beck, M.; Tuttle, B.R.; Schrimpf, R.D.; Fleetwood, D.M.; Pantelides, S.T. Dehydrogenation of defects and hot-electron degradation in Ga<sub>N</sub> high-electron-mobility transistors. *J. Appl. Phys.* **2011**, *109*, 034501. [[CrossRef](#)]
33. Liu, S.-C.; Chen, B.-Y.; Lin, Y.-C.; Hsieh, T.-E.; Wang, H.-C.; Chang, E.Y. Ga<sub>N</sub> MIS-HEMTs with Nitrogen Passivation for Power Device Applications. *IEEE Electron Device Lett.* **2014**, *35*, 1001–1003.
34. Liu, S.-C.; Trinh, H.-D.; Dai, G.-M.; Huang, C.-K.; Dee, C.-F.; Majlis, B.Y.; Biswas, D.; Chang, E.Y. Effective surface treatment for Ga<sub>N</sub> metal-insulator-semiconductor high-electron-mobility transistors using HF plus N<sub>2</sub> plasma prior to Si<sub>3</sub>N<sub>4</sub> passivation. *Jpn. J. Appl. Phys.* **2016**, *55*, 01AD06. [[CrossRef](#)]

35. Zhu, J.; Ma, X.; Hou, B.; Ma, M.; Zhu, Q.; Chen, L.; Yang, L.; Zhang, P.; Zhou, X.; Hao, Y. Comparative Study on Charge Trapping Induced  $V_{th}$  Shift for GaN-Based MOS-HEMTs with and without Thermal Annealing Treatment. *IEEE Trans. Electron Devices* **2018**, *65*, 5343–5349. [[CrossRef](#)]
36. Lu, X.; Jiang, H.; Liu, C.; Zou, X.; Lau, K.M. Off-state leakage current reduction in AlGaIn/GaN high electron mobility transistors by combining surface treatment and post-gate annealing. *Semicond. Sci. Technol.* **2016**, *31*, 055019. [[CrossRef](#)]
37. Lin, S.; Wang, M.; Xie, B.; Wen, C.P.; Yu, M.; Wang, J.; Hao, Y.; Wu, W.; Huang, S.; Chen, K.J.; et al. Reduction of Current Collapse in GaN High-Electron Mobility Transistors Using a Repeated Ozone Oxidation and Wet Surface Treatment. *IEEE Electron Device Lett.* **2015**, *36*, 757–759.
38. Yang, S.; Zheng, Z.; Zhang, L.; Song, W.; Chen, K.J. GaN MIS-HEMTs with Surface Reinforcement for Suppressed Hot-Electron-Induced Degradation. *IEEE Electron Device Lett.* **2021**, *42*, 489–492. [[CrossRef](#)]
39. Mizue, C.; Hori, Y.; Miczek, M.; Hashizume, T. Capacitance–Voltage Characteristics of Al<sub>2</sub>O<sub>3</sub>/AlGaIn/GaN Structures and State Density Distribution at Al<sub>2</sub>O<sub>3</sub>/AlGaIn Interface. *Jpn. J. Appl. Phys.* **2011**, *50*, 021001. [[CrossRef](#)]
40. Yang, S.; Liu, S.; Lu, Y.; Liu, C.; Chen, K.J. AC-Capacitance Techniques for Interface Trap Analysis in GaN-Based Buried-Channel MIS-HEMTs. *IEEE Trans. Electron Devices* **2015**, *62*, 1870–1878. [[CrossRef](#)]